Optical enhancement of the open-circuit voltage in high quality GaAs solar cells

M. A. Steiner,[a] J. F. Geisz, I. García, D. J. Friedman, A. Duda, and S. R. Kurtz
National Renewable Energy Laboratory, Golden, Colorado 80401, USA

(Received 18 January 2013; accepted 6 March 2013; published online 29 March 2013)

The self-absorption of radiated photons increases the minority carrier concentration in semiconductor optoelectronic devices such as solar cells. This so-called photon recycling leads to an increase in the external luminescent efficiency, the fraction of internally radiated photons that are able to escape through the front surface. An increased external luminescent efficiency in turn correlates with an increased open-circuit voltage and ultimately conversion efficiency. We develop a detailed ray-optical model that calculates V_{oc} for real, non-idealized solar cells, accounting for isotropic luminescence, parasitic losses, multiple photon reflections within the cell and wavelength-dependent indices of refraction for the layers in the cell. We have fabricated high quality GaAs solar cells, systematically varying the optical properties including the back reflectance, and have demonstrated $V_{oc} = 1.101 \pm 0.002$ V and conversion efficiencies of $(27.8 \pm 0.8)\%$ under the global solar spectrum. The trends shown by the model are in good agreement with the data. © *2013 American Institute of Physics*. [http://dx.doi.org/10.1063/1.4798267]

I. INTRODUCTION

Spontaneous emission of photons in a solar cell, generated by the radiative recombination of electron-hole pairs, is a fundamental property of semiconductors.[1] Internally emitted photons can escape out the front of the cell as external luminescence, or can be reabsorbed and possibly re-emitted. They can also be absorbed parasitically in non-photoactive layers of the cell and lost. At the open-circuit voltage, V_{oc}, all of the generated electron-hole pairs must recombine within the cell, and in the so-called detailed balance limit,[2] all of the recombination is radiative. In this limit, the total number of externally emitted photons must exactly balance the number of absorbed solar photons, leading to the limiting thermodynamic conversion efficiency of the cell. Thus, an external emission flux that does not exactly balance the absorption indicates a loss mechanism in the cell that leads to a lower V_{oc}. On thermodynamic grounds, several authors[3–5] have shown that the V_{oc} can be expressed as

$$V_{oc} = V_{db} + \frac{kT}{q}\ln(\eta_{ext}), \tag{1}$$

where V_{db} is the ideal open-circuit voltage calculated in the detailed balance limit and η_{ext} is the external luminescent efficiency that quantifies the fraction of internally emitted photons that are ultimately able to escape through the front surface. In the ideal, detailed-balance limit, $\eta_{ext} = 1$ at V_{oc}. The detailed balance limit V_{db} for a specific optical structure can be calculated from the solar spectrum and the external quantum efficiency (EQE),[6,7] because the EQE is a very good approximation for the external absorbance in high quality cells. η_{ext} is related to the self-absorption of photons and is sensitive to the angle- and wavelength-dependent reflectances at the front and back of the cell, as well as the internal luminescent efficiency and the cell thickness, as will be demonstrated. The self-absorption (or recycling) of photons has been studied previously[1,8] and has been shown to increase the equilibrium density of minority carriers, with a corresponding increase in the radiative lifetime. Strong photon recycling effects in GaAs cells with high back reflectance have recently been exploited to dramatically increase the external luminescence,[3,9,10] yielding cells with V_{oc} of 1.122 V and a conversion efficiency of 28.8%.

In the past, several authors[1,8,11,12] modeled the external luminescence, including self-absorption effects, in simpler structures such as AlGaAs/GaAs double-heterostructures. Others described the behavior of idealized single junction solar cells[3,10,13–18] or luminescent concentrator cells.[19] These models make simplifying assumptions, such as: the escape cone at the front is sharp and independent of wavelength, so that the reflectance at the front is zero within the cone and unity outside; the cell is mounted on either a perfect mirror, a completely imperfect-mirror substrate or a layer with a single wavelength-independent index of refraction; there are no parasitic losses in the various layers of the cell; some studies assume that the light makes at most two passes through the cell. These excellent studies outline the physics behind photon recycling but do not lend themselves to a straightforward comparison with real data. In real solar cells, the front and back interfaces are composed of several layers, each with its own set of wavelength-dependent optical constants, so that the reflectances have to be computed with transition matrix algorithms that account for each layer's thickness and optical properties.[20,21] The escape cones at each interface are, in general, wavelength-dependent and thus not sharply defined at a single angle. Moreover, some layers may be absorbing and the related parasitic losses must be considered.

Here, we develop a more comprehensive model that describes the behavior of real solar cells with more complicated, specular reflectance coefficients at each interface. Our model accounts for multiple reflections within the solar cell, and the calculated reflection coefficients include the

[a]email: myles.steiner@nrel.gov

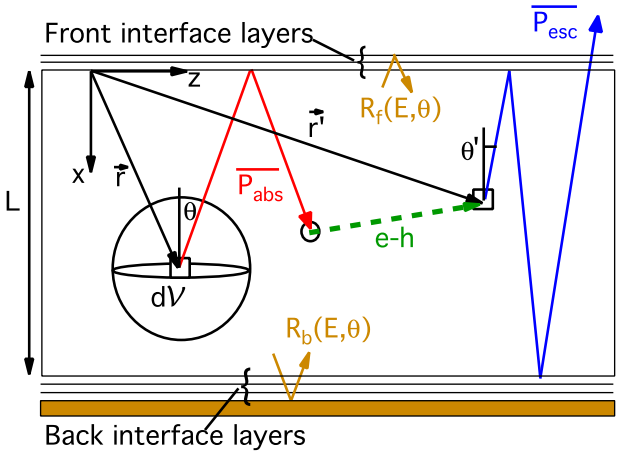

FIG. 1. Geometry for modeling photon recycling. The colored lines represent the different processes that an emitted photon can undergo in the structure: the red line shows a photon emitted at $\vec{r}$ that is re-absorbed after one reflection at the front; the blue line shows a photon emitted at $\vec{r}'$ that escapes after two internal reflections; and the green dashed line represents diffusion of an electron. The yellow arrows at the top and bottom illustrate the effective Fresnel reflection coefficients.

wavelength dependence of the complex indices of refraction for each layer in the cell. The model calculates the probabilities of escape out the front and re-absorption within the cell, integrated over the cell volume, the solid angle of emission, and the distribution over energy. We compare our model to V_{oc} data measured on high-quality GaAs solar cells.

II. MODEL

We follow the optical emission from a single junction solar cell of thickness L and frontal area A, as shown in Fig. 1, to calculate the V_{oc} using Eq. (1). The various assumptions underlying the model are summarized in Table I below. The origin of the coordinate system is on the inside of the front surface, with x directed normal to the surface. Now consider a differential volume element $d\mathcal{V}$ located at position $\vec{r}$ as shown by the small square, and consider the emission from this volume. There are N_{eh} electron-hole pairs per cm^3, and the radiative recombination rate is distributed in energy according to[22]

$$S(E) = \frac{2\alpha(E)n^2(E)E^2}{h^3c^2}\frac{1}{\exp\left(\frac{E-qV}{kT}\right)-1}. \quad (2a)$$

In this expression for the spontaneous emission distribution $S(E)$, $\alpha(E)$ is the absorption coefficient of the absorber layer, $n(E)$ is the index of refraction of the absorber layer, and V is the bias voltage; the other symbols have their usual meanings. For energies $E - qV \gg kT$, the -1 term in the denominator can be neglected, the voltage dependence can be factored out, and we can re-express $S(E)$ as

$$S(E) \approx \frac{2\alpha(E)n^2(E)E^2}{h^3c^2}\exp\left(\frac{-E}{kT}\right)\exp\left(\frac{qV}{kT}\right). \quad (2b)$$

The distribution, normalized by the total number of electron-hole pairs as obtained by integration of $S(E)$ over all the energies, can then be expressed as

$$\hat{S}(E) = \frac{\frac{2\alpha(E)n^2(E)E^2}{h^3c^2}\exp\left(\frac{-E}{kT}\right)\exp\left(\frac{qV}{kT}\right)}{\int_0^\infty S(E)dE}, \quad (2c)$$

and the voltage dependence cancels out.

The internal luminescent efficiency η_{int} is given by

$$\eta_{int} = \frac{U_{rad}}{U_{rad}+U_{nr}}, \quad (3)$$

TABLE I. Assumptions used in the model of V_{oc}, and significant implications, if any.

	Assumption	Justifications and implications
1	Spatially invariant optical parameters $n(E)$ and $\alpha(E)$ in the absorber layer	Doping level is approximately constant; for GaAs cells, both the base and emitter are doped to $\sim 10^{17}$–10^{18} cm^{-3}
2	Spatially uniform distribution of spontaneous emission probability, η_{int}	Minority carrier concentration is uniform, because the diffusion length is very long
3	Solar cell is effectively described by a single-diode model: $J = -J_{sc} + J_{01}\left(e^{\frac{qV}{kT}}-1\right)$	Model neglects non-radiative Shockley-Read-Hall recombination in the depletion region or along the cell perimeter
4	Isotropic emission of photons	Wave optics smeared out by the isotropic nature of emission; only photon intensity remains relevant
5	Ray optics within absorber layer	
6	Reflectance and transmittance for ancillary cladding layers modeled by transfer matrix method	Optical losses in real structures are well-characterized compared to previous work
7	Planar, parallel, and specular interfaces	Model does not account for roughness or texturing of the front or back surfaces (roughness of typical MOVPE-grown solar cells is much less than the wavelength of light)
8	No re-emission of photons from the cladding and contact layers	Model may slightly underestimate the photon recycling for very thick contact layers
9	No shunt conductance	Reasonably good devices only

where U_{rad} and U_{nr} are the radiative and non-radiative recombination rates, respectively. We take η_{int} to be a phenomenological parameter that describes the overall material quality and aggregates the effects of bulk-, interface-, and perimeter-recombination, but in principle, it is a quantum mechanical quantity that could be calculated from the Fermi Golden rule,[23] with knowledge of the various non-radiative recombination trap densities. On average, at V_{oc}, there are

$$\frac{N_{eh} \cdot \hat{S}(E)\eta_{int}}{4\pi} \tag{4}$$

photons per unit volume, time, steradian, and energy emitted from the volume element $d\mathcal{V}$, and we assume the emission is isotropic so that ~50% of the photons are directed upward and ~50% downward. The photon can escape out the front of the cell, either immediately or after several reflections, as exemplified by the blue path in Fig. 1; it can be re-absorbed in the active layer, again either immediately or after several reflections off the interfaces, as shown by the red path in Fig. 1; or it can be re-absorbed parasitically and lost.

We let $P_{esc}(\vec{r}, E, \theta, \phi)$ and $P_{abs}(\vec{r}, E, \theta, \phi)$ represent the probability densities of escape out the front and of re-absorption, respectively, with respect to an initial emission in the differential volume element $d\mathcal{V}$. The direction of emission is defined by the azimuthal angle ϕ and the polar angle θ.

To calculate these quantities in the most general case, the electromagnetic field should be determined at every point by coherent superposition of waves that are emitted from a uniformly distributed set of sources.[24] We make the simplifying assumption that in a uniformly and isotropically emitting volume, any standing wave pattern will ultimately be smeared out so that only the photon intensity remains relevant. Within the cell volume, the photons can, therefore, be treated as non-interacting particles rather than coherent waves. At the specular front and back boundaries, on the other hand, we implicitly retain the wave formulation and calculate the effective Fresnel coefficients by considering the coherent propagation of the electromagnetic waves through the multiple interface layers, using the transfer matrix method as described by Centurioni;[20] similar results are achieved using the algorithm described by Bader.[21] Because the transfer matrix method assumes that the medium from which the light originates is non-absorbing, a difficulty arises: the absorption coefficient of the relevant III-V semiconductor materials is non-zero over the full range of relevant emission wavelengths, and therefore the assumption of a non-absorbing medium does not strictly hold. However, the method can still be applied by effectively separating the absorption in the cell from the reflection at the interface. We then consider the reflection of photons that originate in an infinitesimally thin layer adjacent to the boundary. In that limit, we can justifiably let $\alpha L \to 0$ to calculate the effective Fresnel coefficients. $R_f = R_f(E, \theta)$, $T_f = T_f(E, \theta)$, $R_b = R_b(E, \theta)$, and $T_b = T_b(E, \theta)$ are, therefore, the effective energy- and angle-dependent Fresnel coefficients for specular reflection and transmission at the front and back interfaces, respectively. R_b and R_f are illustrated schematically in Fig. 1.

Physically, $P_{esc}(\vec{r}, E, \theta, \phi)$ represents the probability that a particular photon escapes out the front before it is re-absorbed. If the emitted photon is not absorbed before reaching the front interface, it can be transmitted through that interface and escape, or it can reflect off the front, make a full double pass through the cell and then be transmitted, or reflect and make another pass, etc. Therefore,

$$\begin{aligned} P_{esc}(\vec{r}, E, \theta, \phi) &= \left(e^{-\alpha x/\cos\theta} + e^{-\alpha(L-x)/\cos\theta} R_b e^{-\alpha L/\cos\theta}\right) T_f \times \{1 + R_f R_b e^{-2\alpha L/\cos\theta} + (R_f R_b)^2 e^{-4\alpha L/\cos\theta} + \cdots\} \\ &= T_f \frac{\left(e^{-\alpha x/\cos\theta} + R_b e^{-\alpha(2L-x)/\cos\theta}\right)}{1 - R_f R_b e^{-2\alpha L/\cos\theta}}. \end{aligned} \tag{5}$$

The two terms in the numerator represent the photons emitted toward the front and back surfaces, respectively. We have replaced the vector $\vec{r}$ with the distance x since we anticipate complete translational invariance in the directions parallel to the interfaces; the light that may escape along the cell perimeter, for typical solar cell areas, is neglected.

To calculate $P_{abs}(\vec{r}, E, \theta, \phi)$, which is the probability that a particular photon is re-absorbed,[8] we again note that the photon can be absorbed on the way to the front or back interface, or it can reflect off that interface and then be absorbed, etc.,

$$\begin{aligned} P_{abs}(\vec{r}, E, \theta, \phi) = &\left\{(1 - e^{-\alpha x/\cos\theta}) + e^{-\alpha x/\cos\theta} R_f (1 + e^{-\alpha L/\cos\theta} R_b + e^{-2\alpha L/\cos\theta} R_b R_f + \cdots)(1 - e^{-\alpha L/\cos\theta})\right\} \\ &+ \left\{\left(1 - e^{-\alpha(L-x)/\cos\theta}\right) + e^{-\alpha(L-x)/\cos\theta} R_b (1 + e^{-\alpha L/\cos\theta} R_f + e^{-2\alpha L/\cos\theta} R_b R_f + \cdots)(1 - e^{-\alpha L/\cos\theta})\right\}. \end{aligned} \tag{6}$$

Equations (5) and (6) implicitly include parasitic losses, such as absorption of the luminescence in the non-active layers, through the reflection and transmission coefficients.

To calculate the total probability $P(\vec{r}, E, \theta, \phi)$ that the photon ultimately escapes the cell, recall that a photon can escape directly, or be reabsorbed then re-emitted and escape, or be reabsorbed again, etc.,

$$P(\vec{r},E,\theta,\phi) = \eta_{int}\{P_{esc}(\vec{r},E,\theta,\phi) + P_{abs}(\vec{r},E,\theta,\phi)\eta_{int}\{P_{esc}(\vec{r'},E',\theta',\phi') + P_{abs}(\vec{r'},E',\theta',\phi')\eta_{int}\{P_{esc}(\vec{r''},E'',\theta'',\phi'') + P_{abs}(\vec{r''},E'',\theta'',\phi'')\eta_{int}\{\ldots\}\}\}\}. \quad (7)$$

The various primes designate separate emission events, as illustrated in Fig. 1. In this expression, the values of $(\vec{r},E,\theta,\phi)$ for each absorption term are deliberately matched to the preceding emission term because those probabilities are correlated—emission from the back of the cell is correlated with a higher probability of re-absorption than emission from near the front—but the values for the subsequent emission and absorption are different because those probabilities are uncorrelated with the original probabilities. This can only be true if we assume that the electron-hole pairs can diffuse through the volume with no significant loss so that the spontaneous emission is uniformly distributed through the cell volume. This is a reasonable assumption for high-quality GaAs cells with the junction located close to either the front or back of the absorber layer, but may fail for lattice-mismatched GaInAs cells, for example, or in cells with a strong gradient in the carrier concentration or a strong variation in the density of non-radiative recombination traps. More complicated structures can be accommodated by letting $\eta_{int} = \eta_{int}(\vec{r})$ if the profile is known.

We now integrate the expression over the volume, solid angle, and energy, to find the external luminescent efficiency η_{ext}:

$$\eta_{ext} = \iiint P(\vec{r},E,\theta,\phi)d\vec{r}\,d\vec{r'}d\vec{r''}\ldots dE\,dE'dE''\ldots \times d\Omega\,d\Omega'd\Omega''\ldots. \quad (8)$$

The integrals over the different primes must be independent under the assumption of uniform emission, and the expression reduces to a geometric series

$$\eta_{ext} = \eta_{int}\overline{P_{esc}}\{1 + \eta_{int}\overline{P_{abs}} + (\eta_{int}\overline{P_{abs}})^2 + \cdots\} \quad (9a)$$

or

$$\eta_{ext} = \frac{\eta_{int}\overline{P_{esc}}}{1-\eta_{int}\overline{P_{abs}}}. \quad (9b)$$

$\overline{P_{esc}}$ and $\overline{P_{abs}}$ are volume-, energy-, and solid-angle-averaged probabilities. A similar expression was derived in Refs. 10 and 19 but without a detailed consideration of complicated, multilayer boundaries or more than one internal reflection.

Using Eq. (4) for the total number of emission events per unit volume $d\mathcal{V}$,

$$\overline{P_{esc}} = \frac{\iiint\left\{\frac{N_{eh}\eta_{int}}{4\pi}\int\hat{S}(E)P_{esc}(\vec{r},E,\theta,\phi)sin\theta d\theta d\phi dE\right\}dxdydz}{N_{eh}\eta_{int}\iiint dxdydz}. \quad (10)$$

Since there is no dependence on y or z, $\iint dydz = A$,and the integrals over $\int d\phi = 2\pi$. Using Eq. (5) for $P_{esc}(\vec{r},E,\theta,\phi)$ and carrying out the integration over x explicitly,

$$\overline{P_{esc}} = \int_0^\infty \hat{S}(E)\int_0^{\pi/2}\frac{T_f}{2\alpha L}\frac{(1-e^{-\alpha L/\cos\theta})(1+R_b e^{-\alpha L/\cos\theta})}{1-R_f R_b e^{-2\alpha L/\cos\theta}} \times \cos\theta\sin\theta\,d\theta\,dE. \quad (11)$$

There is a factor of $\cos\theta$ in the angular integral that effectively changes the relative weighting of the emission angles, but notice that it comes from the argument of the exponentials during the integral over dx.

Similarly, using Eq. (6),

$$\overline{P_{abs}} = 1 - \int_0^\infty \hat{S}(E)\int_0^{\pi/2}\left\{\frac{(1-e^{-\alpha L/\cos\theta})}{\alpha L}\left(1-\frac{1}{2}(1-e^{-\alpha L/\cos\theta})\left(\frac{R_f+R_b+2R_fR_be^{-\alpha L/\cos\theta}}{1-R_fR_be^{-2\alpha L/\cos\theta}}\right)\right)\right\}\cos\theta\sin\theta\,d\theta\,dE. \quad (12)$$

The equation is symmetric with respect to an exchange of $R_f \leftrightarrow R_b$, which is not surprising since re-absorption is an internal process that should not preference the direction of external emission. Once again, there is a factor of $\cos\theta$ in the angular integral.

V_{oc} for any solar cell can now be calculated using Eq. (1) with Eqs. (9b), (11), and (12), as long as the optical data are available for each layer to enable an accurate determination of the Fresnel coefficients and the absorption coefficient. Let us observe that while the individual Fresnel coefficients are embedded within these equations, there appears to be no simple functional dependence of V_{oc} on the average reflectance.

III. LIMITING BEHAVIORS

Before comparing the model with data from real solar cells, we briefly consider two limiting cases of the model, which can be compared with the literature. Calculations of the probabilities $\overline{P_{esc}}$, $\overline{P_{abs}}$, and η_{ext} for a range of absorber-layer thicknesses (i.e., emitter + base) are shown in Fig. 2. The black curves are based on a specific but representative

GaAs cell structure, with a high back reflectance, that is illustrated in Fig. 3 and described in Sec. IV. The curves, therefore, show the calculation of these probabilities for a real GaAs solar cell using wavelength-dependent optical data for each layer. The red and green curves show the calculation for a pair of simpler, idealized solar cells, modeled as follows: the idealized cells have thickness L, a wavelength-independent index of refraction n, a wavelength-independent absorption coefficient α_0, and no absorption below the bandgap. For the curves in Fig. 2, n and α_0 were taken from the optical properties of GaAs at 873 nm, the wavelength at which $S(E)$ is a maximum. The front reflectance is $R_f = 1 - T_f = \begin{cases} 0 : \theta < \theta_c \\ 1 : \theta > \theta_c \end{cases}$, where the critical angle θ_c is defined by $\sin\theta_c = 1/n$. The back reflectance is $R_b(E,\theta) = 0$ for the red curves, representing a perfect photon sink such as an absorbing substrate, and $R_b(E,\theta) = 1$ for the green curves, representing a perfect back reflector.

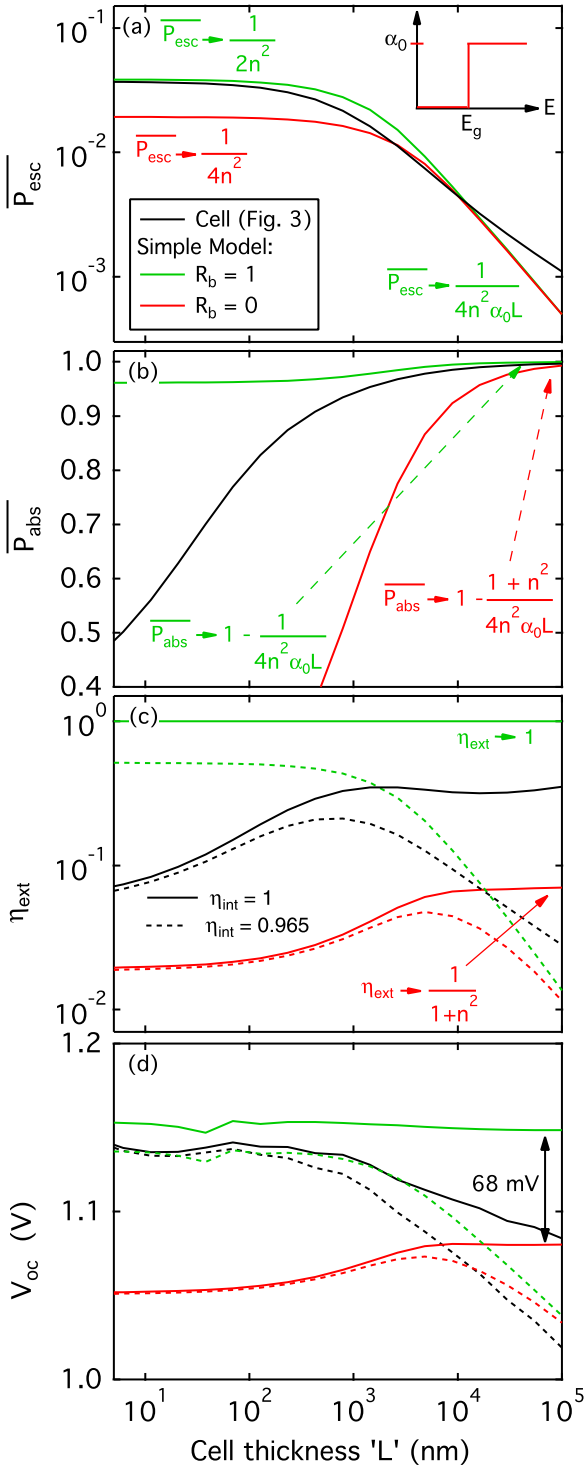

FIG. 2. Calculation of $\overline{P_{esc}}$, $\overline{P_{abs}}$, η_{ext}, and V_{oc} for a representative GaAs cell structure with a high back reflectance (black), and for a pair of simpler, idealized cells with a step-function absorption coefficient and with $R_b = 1$ (green) and $R_b = 0$ (red); the idealized absorption coefficient is illustrated in the upper-right inset to (a). Limiting expressions for the idealized cells are also shown, derived from Eqs. (11) and (12): $n = 3.65$ is the refractive index, $\alpha_0 = 0.47\,\mu\text{m}^{-1}$ is the absorption coefficient, and L is the absorber thickness. In (c) and (d), the solid lines are for $\eta_{int} = 1$ and the dashed lines for $\eta_{int} = 0.965$.

In the strong absorption limit, defined by $e^{-\alpha_0 L/\cos\theta} \approx 0$, Eq. (11) for $\overline{P_{esc}}$ reduces to

$$\overline{P_{esc}} \to \frac{1}{4n^2\alpha_0 L} : R_b = 0 \text{ or } 1, \tag{13}$$

for both $R_b = 0$ and $R_b = 1$. These trends are illustrated on the right side of Fig. 2(a), at large values of the cell thickness L. This limit makes physical sense because as L increases, a higher fraction of the photons are emitted from deep within the cell and are likely to be re-absorbed before reaching the front surface, and therefore do not escape. Correspondingly, Eq. (12) for $\overline{P_{abs}}$ reduces to

$$\overline{P_{abs}} \to \begin{cases} 1 - \dfrac{1}{4n^2\alpha_0 L} : R_b = 1 \\ 1 - \dfrac{1+n^2}{4n^2\alpha_0 L} : R_b = 0 \end{cases} \tag{14}$$

both of which increase with L, as shown in Fig. 2(b).

Over the entire thickness range, $\overline{P_{esc}}$ is $\leq 3.8\%$ for all three curves in Fig. 2(a), indicating a low probability that an emitted photon can directly escape. This may seem counter-intuitive at first, since most photons are emitted near the band-edge where the absorption is relatively weak. However, most

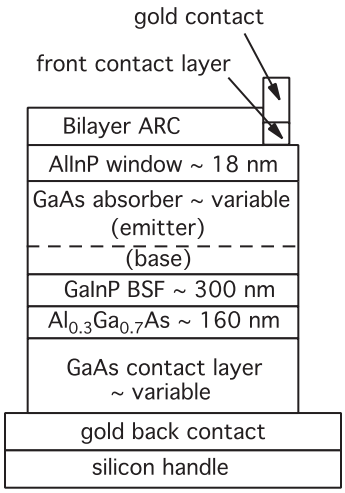

FIG. 3. Schematic (not to scale) of the GaAs solar cells studied here. The thicknesses are nominal. The silicon handle is bonded during processing to provide mechanical stability. The dashed line represents the *pn* junction.

of those photons are emitted outside of the escape cone of the front surface and strike the front interface at angles where they are totally internally reflected. Indeed, the angular weighting in Eq. (11) favors angles near 45°, outside the escape cone, rather than angles close to normal. Thus, the fraction of emitted photons that can escape directly is indeed low.

Using the limiting forms in Eqs. (13) and (14), and assuming an internal luminescent efficiency of $\eta_{int} = 1$, the limiting values of η_{ext} are

$$\eta_{ext} \rightarrow \begin{cases} 1 & : \quad R_b = 1 \\ \dfrac{1}{1+n^2} & : \quad R_b = 0, \end{cases} \tag{15}$$

shown in Fig. 2(c). With both front and back reflectances of unity and with perfect material quality, there are no losses in the cell within the assumptions of this model, and therefore all internally emitted photons must eventually escape so that $\eta_{ext} \rightarrow 1$ and $V_{oc} = V_{db}$. For this reason, this limit can also be derived from Eqs. (11) and (12) in the more general case, where $\alpha(E)$ is wavelength-dependent. With $R_b = 0$, on the other hand, photons that strike the back surface are lost, and the external luminescence is therefore diminished, a relationship derived (in a slightly different form) by Henry.[17] Using $n = 3.6$ for GaAs, $\eta_{ext} \sim 0.072$ for this case, and we find $V_{oc} \approx V_{db} - 68\,\text{mV}$ using Eq. (1). We expect V_{db} to decrease slightly as the optics improve and the absorbance increases,[6] but most of the 68 mV accrues to V_{oc}. This provides an estimate for the maximum improvement in V_{oc} that may be expected from enhancing the optics in high quality cells. Both η_{ext} and V_{oc} will decrease as η_{int} decreases from unity, and the magnitude of these quantities for the two cases of $R_b = 0$ and $R_b = 1$ will tend to converge at large thicknesses, as shown for example by the dashed lines in Figs. 2(c) and 2(d) for $\eta_{int} = 0.965$.

The opposite, weak absorption limit of $\overline{P_{esc}}$ can also be evaluated analytically. This limit is defined by $e^{-\alpha_0 L/\cos\theta} \approx 1 - \alpha_0 L/\cos\theta$, and Eq. (11) reduces approximately (for $n > 1$) to

$$\overline{P_{esc}} \rightarrow \begin{cases} 1/2n^2 : R_b = 1 \\ 1/4n^2 : R_b = 0, \end{cases} \tag{16}$$

which correspond to the intensity enhancement factors due to angle-averaging and volume absorption that were derived in Ref. 16 for textured solar cells.

The behavior of the full cell structure illustrated in Fig. 3, which is computed by averaging over all wavelengths and is shown in black on all four plots in Fig. 2, does not follow either limiting case exactly. At small thicknesses, the cell follows $R_b = 1$ for $\overline{P_{esc}}$ and neither case for $\overline{P_{abs}}$. At large thicknesses, the cell approaches the $R_b = 1$ behavior for $\overline{P_{abs}}$, and exceeds both cases for $\overline{P_{esc}}$. We will return to this figure after discussing the data.

IV. EXPERIMENTAL DETAILS

Figure 3 shows the nominal structures of the n/p GaAs solar cells studied here. The front of the emitter is passivated with an AlInP window layer and covered with a bilayer anti-reflection coating. Most of the cells were grown with the junction located very near the back, so that the emitter constitutes the majority of the active region. The emitter was n-type doped to $\sim 10^{17}\,\text{cm}^{-3}$. Behind the thin base layer, a GaInP barrier layer (commonly denoted as the back surface field, or BSF) helps confine minority carriers in the base, and a highly doped $Al_{0.3}Ga_{0.7}As$/GaAs back contact layer enables ohmic contact with the rear contact metal, in this case electroplated gold. Varying the internal optics can be accomplished by (1) varying the thickness of the optically absorbing GaAs back contact layer, which changes the reflectance $R_b(E, \theta)$; (2) varying the thickness of the cell; (3) changing the anti-reflection coating or window layer thickness, which changes $R_f(E, \theta)$.

Cells were grown by atmospheric pressure metal-organic vapor-phase epitaxy (MOVPE) in a custom-built vertical reactor. Growth conditions are described elsewhere.[25] The morphology of the growth surface was specular and defect-free, justifying the assumption that the various interfaces are planar and specular. Dopants were derived from triethylzinc, carbon tetrachloride, and hydrogen selenide. The nominal n-type doping in the thick emitter layer was $\sim 10^{17}\,\text{cm}^{-3}$. All samples were grown inverted, with the emitter grown before the base, and then flipped and mounted on a silicon handle during processing. The inverted growth technique allows for direct access to the rear contact layer for efficient deposition of a reflective mirror. Cells were processed using standard photolithographic techniques to define cell areas of 0.25 cm^2, with ~2% shadowing from the metal grids and contact pad. The 50-nm ZnS and 100-nm MgF_2 anti-reflection coating layers were deposited by thermal evaporation.

External quantum efficiency was measured on a custom instrument with a 270-mm monochromator and a tungsten-halogen lamp, in 5-nm steps. Current-voltage characteristics were measured on a class A solar simulator with a xenon lamp. A calibrated GaAs reference cell, in conjunction with a spectral mismatch correction factor,[26] was used to set the light intensity to the equivalent of the ASTM G173 global reference spectrum at 1000 W/m^2. All measurements were taken at 25 °C. The optical data, comprised of the index of refraction and the absorption coefficient, have been measured by spectroscopic ellipsometry and transmission for most layers, or taken from the literature.[27]

V. RESULTS AND DISCUSSION

Figure 4 shows maps of the modeled reflectance at the GaAs/GaInP-BSF interface (hereafter referred to as back reflectance) for two thicknesses of the GaAs contact layer, for the structure in Fig. 3. The red region near the top of both maps shows that there is total internal reflection at some angle for every wavelength, because the index of refraction of the BSF layer is lower than the index of GaAs. For the thin contact layer, the reflectance exceeds 93% near the bandedge for all angles, whereas for the thicker contact layer, the reflectance drops to ~55%–75% for angles less than 65°. The fine structure in both maps results from interference effects in the BSF-AlGaAs-GaAs-Au layers.

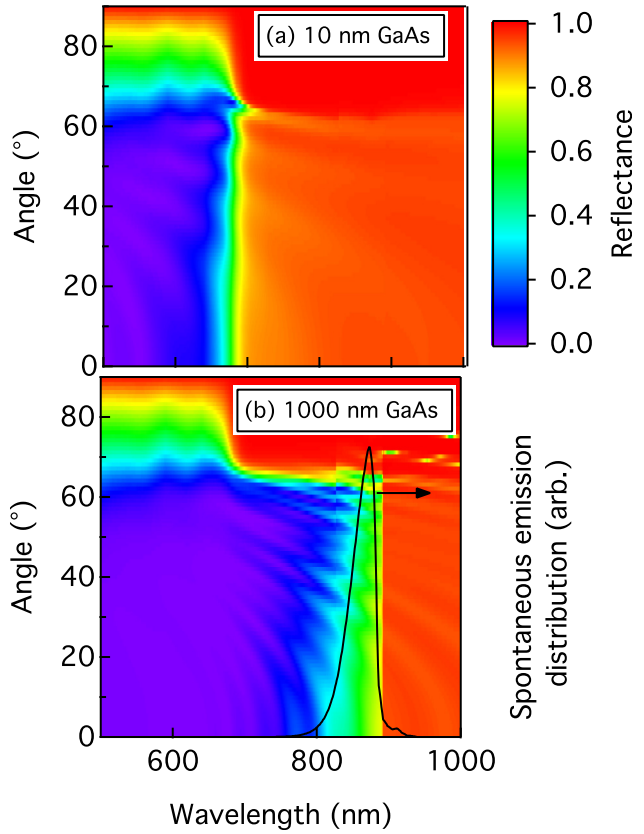

FIG. 4. Back-reflectance maps as a function of angle and wavelength, for different thicknesses of GaAs back contact layer: (a) 10 nm and (b) 1000 nm. In both cases, the cell thickness was 2 μm. The Fresnel reflectance for each angle and wavelength is calculated at the GaAs-GaInP interface at the back of the absorber. The black curve in (b) shows the shape of the spontaneous emission distribution.

Before discussing the cell results, let us digress for a moment to note that, in principle, it is important that the same optical structure be used to calculate both V_{db} (the V_{oc} in the radiative limit as discussed earlier) and η_{ext} in Eq. (1). While V_{db} can be calculated directly from the measured EQE,[6] the actual layer thicknesses in the device are unlikely to exactly match the nominal design thicknesses. Indeed, wafer maps of GaAs and GaInP epilayers grown on our reactor show a typical variation of ~5% in the film thickness. In practice, this level of variation will only change the modeled values of V_{oc} by a few millivolts. Nevertheless, the analysis can be improved by modeling the QE and then calculating both V_{db} and η_{ext} from the model. An algorithm for modeling the absorbance in the cell layers, and thus the ideal QE with no electrical losses, was described by Centurioni[20] and is used in the model presented here. With respect to the monochromatic incident light, the cell is just a Fabry-Perot cavity in a lossy medium, in which the damped forward-traveling light waves interfere coherently with damped reflected light waves to produce a standing wave pattern as a function of the depth. The complex reflection and transmission amplitudes must be calculated at each interface.

Figure 5 shows an example of a measured QE for a 2-μm-thick cell with a 10-nm-thick GaAs back contact layer. The actual layer thicknesses were determined from the optical fit and were within 5% of the nominal values. Also

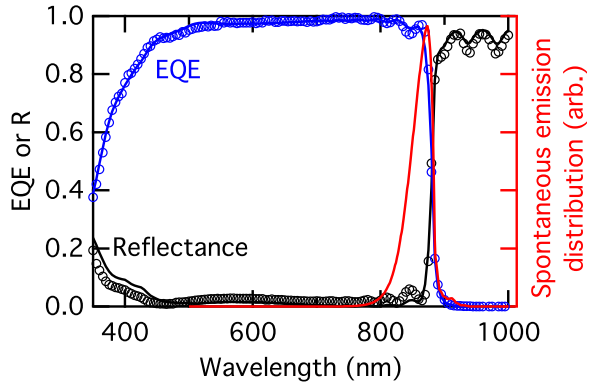

FIG. 5. Measured (points) and modeled (lines) EQE and reflectance for a GaAs cell. The various layer thicknesses were adjusted from the nominal values, based on ~5% variations in the growth rate, to give a good fit. The red curve shows the spontaneous emission distribution, where the QE data are most important for the V_{oc} model.

shown is the spontaneous emission distribution, calculated from Eq. (2), that shows the wavelengths near the bandedge that dominate the V_{oc} model.

In Fig. 6, we show the measured and modeled V_{oc} data for five samples with varying thicknesses of the GaAs contact layer; the left-most data points are described by the QE in Fig. 5, which is also the basis for the modeling in Fig. 2. We have included the measured data for multiple devices on each sample. The V_{oc} decreases monotonically, though nonlinearly, with the GaAs back-contact layer thickness because the increased absorption of the luminescence in this layer leads to a reduced reflectance at the back of the cell, as shown in Fig. 4.

The modeled behavior for six values of the internal luminescent efficiency η_{int} are also shown. The roughness in each line is not noise, but rather comes from the fine sensitivity of V_{db} to the back contact thickness as shown by the dashed line. V_{db} increases slightly with the contact thickness because of the decreasing external absorbance,[6] which occurs because

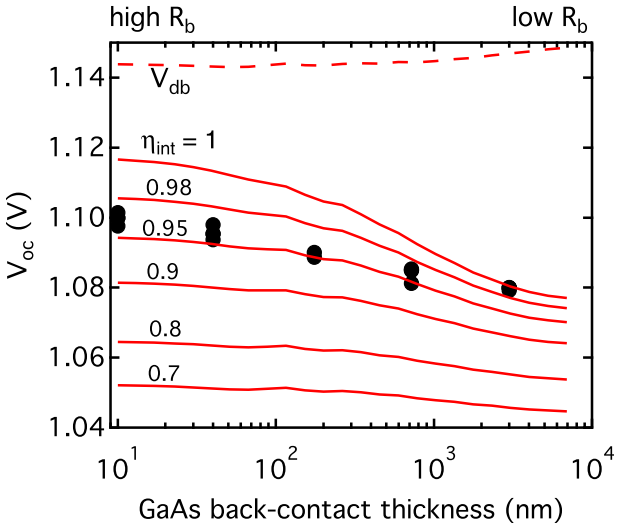

FIG. 6. Modeled (lines) and measured (points) behavior of V_{oc} for structures with varying thickness of the back contact layer. The active layer thickness was nominally 2 μm. The solid red lines represent different values of the internal luminescent efficiency η_{int}. The dashed line at the top shows the modeled V_{db}.

thin cells rely on the back reflectance to increase the probability that an incident solar photon will make multiple passes through the cell, and therefore a lower back reflectance effectively reduces the optical thickness.

Similar to the data, the model shows a decrease in V_{oc} with increasing GaAs back contact thickness. As η_{int} decreases from unity, the curves shift downward and become less sensitive to the back contact thickness. This trend illustrates the increasing returns offered by good material quality. The curves all tend to level out at large contact thicknesses, as expected. We note that at large thicknesses, equivalent to the case of an on-substrate cell without enhanced rear optics, $V_{oc} > 1.06$V even for $\eta_{int} = 0.9$, and as high as $V_{oc} \sim 1.075$V for $\eta_{int} = 1$. The opposing trends in V_{oc} and V_{db} clearly demonstrate the significant role that the external luminescence η_{ext} plays in determining V_{oc}, regardless of the value of η_{int}, and are consistent with the limiting values of Eq. (15) that show a decreasing η_{ext} as the back reflectance decreases.

The data generally follow the modeled trends and are consistent with $\eta_{int} = 0.965$, with some variation as may be expected from a series of independent growths. Let us note that we have neglected any re-emission of absorbed photons in the back contact layer. Some of the electron-hole pairs created there may indeed recombine radiatively, though we expect most to quickly recombine non-radiatively at the GaAs-Au interface. As the contact thickness increases, however, the relative influence of that carrier sink will diminish, and the re-emitted photons will tend to have a small, positive, effect on V_{oc}. This, rather than random variation, may explain why the data at the 3-μm back contact thickness have a higher value than expected.

In the detailed balance limit, where $\eta_{ext} = 1$, Eq. (1) shows that $V_{oc} = V_{db}$, but for the specific structure modeled here, $V_{oc} < V_{db}$ even for $\eta_{int} = 1$ because there are optical parasitic losses at the interfaces, through imperfect reflection and transmission. Indeed, the general inequality $V_{oc} \leq V_{db}$ implies $\eta_{ext} \leq 1$ in Eq. (1), and setting $\eta_{int} = 1$ in Eq. (9) leads to the condition that

$$\overline{P_{abs}} + \overline{P_{esc}} \leq 1 \tag{17}$$

with equality only achieved in the limit where there are no parasitic losses.

The calculated values of V_{db}, $\overline{P_{esc}}$, $\overline{P_{abs}}$, and η_{ext}, with $\eta_{int} = 0.965$, are shown in Table II for modeled cells corresponding to the data of Fig. 6. For the highest reflectance sample (10 nm contact), $\overline{P_{abs}} + \overline{P_{esc}} \approx 0.975$, indicating less than 3% optical parasitic loss, and yet η_{ext} is only $\sim$0.176, as illustrated by the dashed black line in Fig. 2(c) at a thickness of 2 μm. With $\eta_{int} = 1$, this would still only increase to $\sim$0.344. We, therefore, see clearly that η_{ext} depends strongly on all the optical and electrical parasitic losses.

As the contact layer gets thicker and more radiated light is lost from the active layer population by absorption there, the reflectance at the back correspondingly decreases and both $\overline{P_{esc}}$ and $\overline{P_{abs}}$ decrease. The values of $\overline{P_{esc}}$ are all $\leq$1.3%, indicating a very low probability that an emitted photon can directly escape out the front of the cell, as discussed earlier in Sec. III. $\overline{P_{abs}}$ exceeds 96% for the most reflective back contact and only decreases to 86.2% for the least reflective, 3 μm thick contact. Even with this heavily absorbing contact, on average 86.2% of radiative recombination events lead to reabsorption. In the limit of a semi-infinite contact layer, $\overline{P_{abs}}$ is still 82.3% as shown in the last row of Table II. Therefore, there is a considerable amount of photon recycling even in cells with no enhanced optics, and we expect that on-substrate GaAs cells of comparable material quality to these should have $V_{oc} = 1.071$ V. This represents a voltage difference of $V_{oc} - V_{db} = 80$ mV. With perfect material quality, the upright, on-substrate cell should be limited to 1.076 V with this structure, and $V_{oc} - V_{db} \approx 75$ mV, slightly greater than the approximation of 68 mV in Sec. III, calculated for an idealized structure with $\eta_{int} = 1$.

Figure 7 shows measured and modeled V_{oc} data for a second set of cells where the thickness of the active layer was varied from $\sim$1–3.5 μm. For these cells, the GaAs contact layer at the back of the cell was eliminated and the gold contact was electroplated directly to the heavily doped AlGaAs layer. For all of the these cells, the back reflectance is very high, since the AlGaAs has a nominal bandgap of 1.66 eV, above the wavelength of the GaAs bandedge luminescence, and therefore the reflectance of GaAs-emitted light from the back surface is relatively unaffected by absorption in that layer. Also shown for comparison, in green and blue, are data and fits for two other sets of cells with slightly different layer structures, doping profiles, and material quality.

The red dashed lines show modeled V_{oc} for cells corresponding to the red data points. The model shows that V_{oc} should decrease with increasing thickness for any value of η_{int}. The red data, by contrast, show V_{oc} to remain approximately constant with increased cell thickness, which implies that the internal luminescent efficiency must actually increase with thickness for this set of samples; $\eta_{int} \sim 0.9$ for

TABLE II. Modeled values for the data in Fig. 6, using $\eta_{int} = 0.965$. V_{db} is calculated from Ref. 6, all other values are calculated from Eqs. (1), (9), (11), and (12). The bottom row shows the calculated values for the same cell with a semi-infinite contact layer. The final column shows the measured V_{oc} for the best device of each sample.

GaAs back contact thickness (nm)	V_{db} (V)	$\overline{P_{esc}}$	$\overline{P_{abs}}$	η_{ext}	V_{oc} (V)	Measured V_{oc} (V)
10	1.144	0.0131	0.962	0.176	1.099	1.101
40	1.144	0.0129	0.959	0.168	1.098	1.098
175	1.144	0.0128	0.945	0.140	1.093	1.090
720	1.144	0.0124	0.912	0.100	1.085	1.085
3000	1.147	0.0113	0.862	0.0649	1.076	1.080
∞	1.151	0.00944	0.823	0.0443	1.071	…

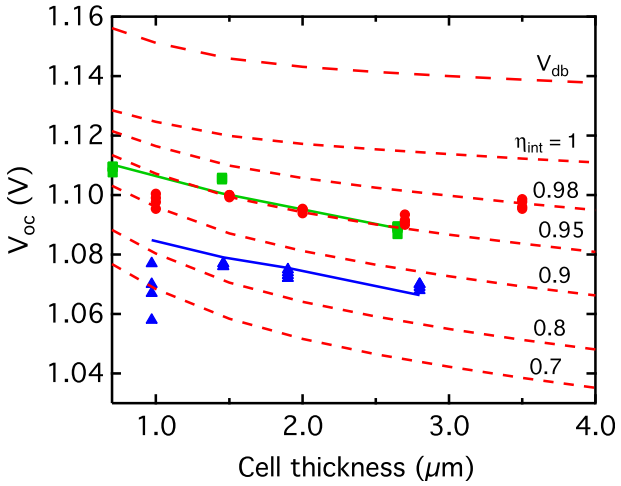

FIG. 7. Modeled (red lines) and measured (red points) behavior of V_{oc} for structures with varying thickness of the active layer. The back contact consisted only of $Al_{0.3}Ga_{0.7}As$ (i.e., no GaAs layer). The dashed lines represent different values of the internal luminescent efficiency η_{int}. The dashed line at the top shows the calculated value of V_{db}. The blue and green points show results for cells with slightly different structures from the red data, modeled with internal luminescent efficiencies of 0.88 and 0.95, respectively.

the thinnest cells, increasing to $\eta_{int} \sim 0.98$ for the thickest. The measured sheet conductance (not shown) varies linearly with the emitter thickness, implying that the majority carrier concentration is approximately the same for all five samples. η_{int}, however, is sensitive to minority carrier recombination, which may vary from sample to sample even as the majority carrier concentration remains constant.

We chose to present these data, despite the small inconsistency with the expected values, because they reinforce a truism about minority carrier devices: the open-circuit voltage is arguably the best probe of the internal quantum efficiency, and therefore the overall material quality, because it aggregates all other internal effects. It can be measured very accurately and can be measured on the actual device rather than on similar test structures. Without the model in Fig. 7, one would have concluded that a flat V_{oc} trend indicates constant material quality, when in fact it appears to indicate a relative improvement in the material quality with thickness. Such an improvement could arise from the diminishing influence of non-radiative recombination at the back interface, for example.[28]

As shown in Fig. 5, having an accurate model of the QE that can be used to calculate the quantities in Eqs. (1) and (9) is useful for demonstrating trends as the cell geometry changes. The same model and calculation can be used to estimate the expected distribution of the V_{oc}s for a large set of cells, due to statistical variation in the layer thicknesses, for example. Uniformity maps of GaAs and GaInP epilayers typically show a ~5% standard deviation in thickness across the wafer. The distribution of V_{oc} about a nominal value can be determined from a Monte Carlo simulation, as follows: we simulate some number of similar cells where for each cell, the thickness of each layer is randomly drawn from a normal distribution with 5% standard deviation about the nominal thickness for that layer. We then calculate V_{db} and η_{ext} for each cell and use Eq. (1) to find V_{oc}, and then plot a histogram of the results for the ensemble. Fig. 8 shows a histogram of V_{oc} for the cell in Fig. 5, for 1000 members of the ensemble. The mean of the distribution coincides with the calculated value for the nominal structure. The standard deviation is ~1 mV, and 95% of the data lie within ±2.15 mV of the mean. This distribution is generally consistent with the observed spread in the data in Figs. 6 and 7.

In Fig. 9, we show the JV curve for our best cell fabricated to date. This particular cell is 2 μm thick with a 10-nm GaAs back contact layer (leftmost data points in Fig. 6, and first row of Table II), even though we would have

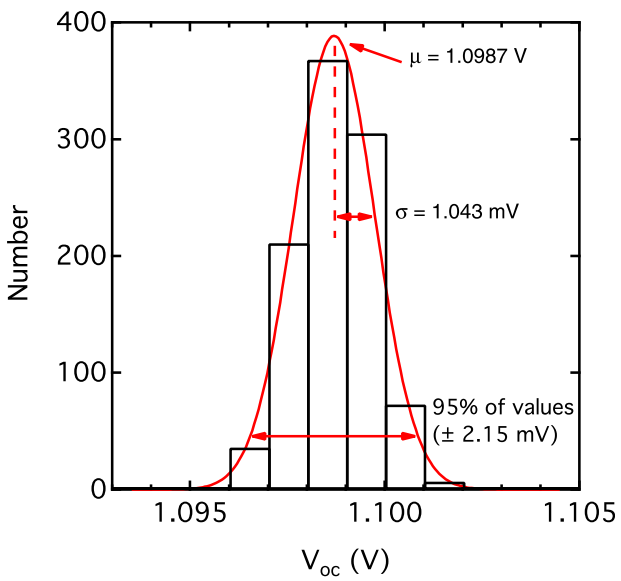

FIG. 8. V_{oc} distribution for a 2 μm cell with 10 nm GaAs back contact layer, assuming 5% variation in thickness for all grown layers. The histogram is based on 1000 simulations, and the data are binned in 1 mV intervals. The fit is Gaussian.

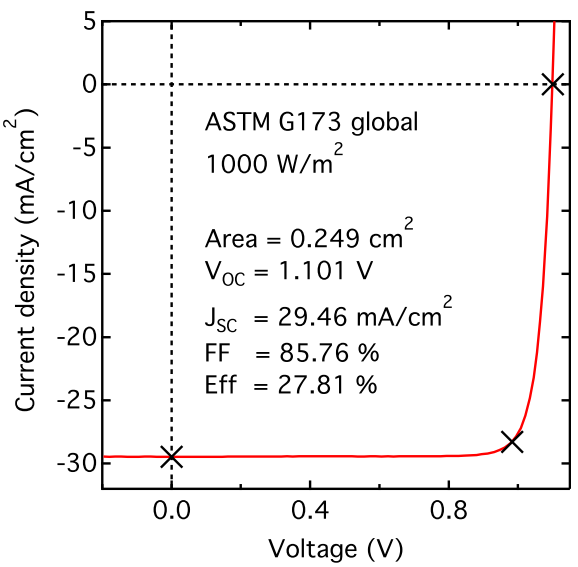

FIG. 9. JV curve for a 2 μm thick cell with 10 nm GaAs back contact layer, under the G173 global spectrum at 1000 W/m². The X symbols denote V_{oc}, J_{sc}, and the maximum power point.

expected slightly better results for a cell with no GaAs in the contact layer. The external luminescence efficiency was calculated to be ~17.6%, as shown in Table II. Official measurements at NREL show a V_{oc} of 1.101 ± 0.002 V and conversion efficiency under the ASTM G173 global spectrum of $(27.8 \pm 0.8)\%$.

VI. CONCLUSIONS

Several general conclusions can be drawn from the model and data presented here. First, the external luminescence depends on both the overall material quality of the absorber layer, including the electronic quality of the interfaces, and on the parasitic optical losses in the front and back interface layers. These losses may be only a few percent and yet have a large effect on η_{ext} because the emitted photons bounce multiple times off the interfaces. Indeed, we find η_{ext} as low as ~4% even though $\overline{P_{abs}}$ exceeded 80% for all of the GaAs cells studied here.

Second, the trends in Fig. 6 show the enhanced voltage available from both high internal luminescent efficiency and high back reflectance. With low material quality (i.e., low η_{int}), V_{oc} is relatively insensitive to the back reflectance: for the GaAs cells modeled here, V_{oc} increased by ~5 mV with $\eta_{int} = 0.7$ over the range of reflectances. With high material quality, on the other hand, the V_{oc} increase was ~40 mV. Therefore, in cells where the material quality is relatively poor, it may not be worth the effort to improve the reflectance, but in systems with good material quality, there are significant voltage and efficiency gains available if the reflectance can be improved. The model presented here provides a formalism for evaluating these gains quantitatively.

Third, while a highly simplified model of a solar cell—one with a step-function absorption coefficient and wavelength-independent front and back reflectances—allows for a rough estimate of the external luminescence in the limits of either completely perfect or completely imperfect reflectances, the demonstrated sensitivity of η_{ext} to the parasitic losses and the material quality indicate that the full numerical calculation presented here is required for an accurate determination of η_{ext} in a specific structure.

Finally, the model is a useful tool for exploring design changes that may improve the cell efficiency, for example, by using different metals or dielectric/metal combinations for the back reflector and different dielectrics in the anti-reflection coating on the front of the cell, and by optimizing the various semiconductor layer thicknesses. More complicated structures can also be studied by relaxing some of the assumptions in the model. For example, a non-uniform carrier distribution or semiconductor composition can be accommodated by letting $\eta_{int} = \eta_{int}(\vec{r})$ and $\alpha(E) = \alpha(E, \vec{r})$ if the profile is known, and then numerically carrying out the integrals over $d\vec{r}$ in Eqs. (7) and (8). As another example, the significant front grid coverage for a concentrator cell can be included by separately calculating the Fresnel coefficients $R_f(E, \theta)$ for the regions under the metal and away from the metal, and then taking a weighted average of the two values. Additional modifications to the equations may be necessary to account for electrical effects, such as depletion region or perimeter recombination, or for the optical effects of texturing of either surface, which could be useful for boosting the photocurrent in thin cells.

In summary, we have developed a mathematical model to calculate V_{oc} for real solar cells with substantial photon recycling processes and non-negligible parasitic losses. The model accounts for isotropic luminescent emission within the cell, and averages over the numerous passes that a photon may take through the cell. We find good agreement with the trends in data measured on high quality GaAs solar cells. The probability that a luminescent photon is re-absorbed is found to exceed 80% even for cells on the substrate with no enhanced back reflection, and to exceed 96% for cells with very good rear optics. The probability that the photon escapes directly out the front, without being re-absorbed, is only $\sim 1\% - 2\%$. The model can be applied to any solar cell for which the index of refraction and the absorption coefficient are well characterized for each layer, and can be adapted to more complicated multijunction solar cells with emission from more than one layer.

ACKNOWLEDGMENTS

The authors are grateful for conversations with E. Yablonovitch, C.-S. Ho, R. King, J. Olson, B. McMahon, R. France, and O. Miller. We thank W. Olavarria and M. Young for dedicated work growing and fabricating the cells; S. Choi for ellipsometry measurements of III-V films; and K. Emery, T. Moriarty, and R. Williams for the JV measurements. I. García holds a Fulbright postdoctoral scholarship funded by the Spanish Ministerio de Educación, by means of the Programa Nacional de Movilidad de Recursos Humanos del Plan Nacional de I-D+i 2008-2011. Research was supported by the U.S. Department of Energy under Contract No. DE-AC36-08GO28308 with the National Renewable Energy Laboratory and funded by the Foundational Program to Advance Cell Efficiency (F-PACE).

[1]E. Yablonovitch, T. J. Gmitter, and R. Bhat, Phys. Rev. Lett. **61**, 2546 (1988).
[2]W. Shockley and H. J. Queisser, J. Appl. Phys. **32**, 510 (1961).
[3]O. D. Miller, E. Yablonovitch, and S. R. Kurtz, J. Photovolt. **2**, 303 (2012).
[4]R. T. Ross, J. Chem. Phys. **45**, 1 (1966).
[5]U. Rau, Phys. Rev. B **76**, 085303 (2007).
[6]E. S. Toberer, A. C. Tamboli, M. Steiner, and S. Kurtz, in *38th IEEE Photovoltaic Specialists Conference* (IEEE, Austin, TX, 2012).
[7]M. A. Green, Prog. Photovolt. **20**, 472 (2012).
[8]P. Asbeck, J. Appl. Phys. **48**, 820 (1977).
[9]B. M. Kayes, H. Nie, R. Twist, S. G. Spruytte, F. Reinhardt, I. C. Kizilyalli, and G. S. Higashi, in *37th IEEE Photovoltaic Specialists Conference* (IEEE, Seattle, WA, 2011), p. 4.
[10]O. D. Miller, Ph.D. dissertation, University of California, Berkeley, 2012.
[11]R. K. Ahrenkiel, B. M. Keyes, G. B. Lush, M. R. Melloch, M. S. Lundstrom, and H. F. Macmillan, J. Vac. Sci. Technol. A **10**, 990 (1992).
[12]I. Schnitzer, E. Yablonovitch, C. Caneau, and T. J. Gmitter, Appl. Phys. Lett. **62**, 131 (1993).
[13]J. L. Balenzategui and A. Marti, Sol. Energy Mater. Sol. Cells **90**, 1068 (2006).
[14]A. Marti, J. L. Balenzategui, and R. F. Reyna, J. Appl. Phys. **82**, 4067 (1997).
[15]A. Marti and G. L. Araujo, Sol. Energy Mater. Sol. Cells **43**, 203 (1996).
[16]E. Yablonovitch and G. Cody, IEEE Trans Electron Devices **ED-29**, 300 (1982).

[17]C. H. Henry, J. Appl. Phys. **51**, 4494 (1980).
[18]X. Wang, M. R. Khan, J. L. Gray, M. A. Alam, and M. S. Lundstrom, J. Photovolt. **3**, 737 (2013).
[19]J. S. Batchelder, A. H. Zewail, and T. Cole, Appl. Opt. **18**, 3090 (1979).
[20]E. Centurioni, Appl. Opt. **44**, 7532 (2005).
[21]G. Bader, P. V. Ashrit, F. E. Girouard, and V.-V. Truong, Appl. Opt. **34**, 1684 (1995).
[22]J. I. Pankove, *Optical Processes in Semiconductors* (Dover Publications, Inc, New York, 1975).
[23]W. v. Roosbroeck and W. Shockley, Phys. Rev. **94**, 1558 (1954).
[24]A. Niv, M. Gharghi, C. Gladden, O. D. Miller, and X. Zhang, Phys. Rev. Lett. **109**, 138701 (2012).
[25]J. F. Geisz, S. R. Kurtz, M. W. Wanlass, J. S. Ward, A. Duda, D. J. Friedman, J. M. Olson, W. E. McMahon, T. Moriarty, and J. Kiehl, Appl. Phys. Lett. **91**, 023502 (2007).
[26]C. R. Osterwald, K. A. Emery, D. R. Myers, and R. E. Hart, in *21st IEEE Photovoltaic Specialists Conference* (IEEE, Kissimmee, FL, 1990), p. 1062.
[27]See http://www.sspectra.com/sopra.html for SOPRA database, 2013.
[28]S. R. Kurtz, P. Faine, and J. M. Olson, J. Appl. Phys. **68**, 1890 (1990).